## 5.1 Introduction

In this chapter the fabrication steps and the optical characterization of the devices previously proposed will be presented. Firstly, the necessary experimental setups in order to measure the power losses, the wavelength response and the modal profile will be briefly described. Then, each device will be treated separately, showing its fabrication steps, together with its characterization. For clarification, a single chip will be drawn on each photolithographic step. It has to be noted, however, that neither the dimensions are accurate nor the mask is only formed by the shown scheme.

## 5.2 Experimental setups

The measurement of integrated optical devices is the final step on the characterization process. Actually, simulation and fabrication steps can only be validated when experimental results match with these of the simulations. Basically, all measurement setups have the same configuration: a light source, a positioning system and a readout method. By light injection it is understood both the light source and the coupling to the optical fiber. The positioning system, either for the fiber optics and for the sample to be measured consists on measuring stages. Finally, the detection mechanism significantly varies depending on the measurement to be done: it can be either a photodetector or a CCD camera.

Light injection from the fiber optics to the sample to be measured has been done using the *end-fire coupling*, which basically consists on direct heading of the fiber optics to the device. This method is commonly used in integrated optics. Nevertheless, it requires extremely accurate positioning system. As can be observed in fig 5.1, it is achieved by two ways: firstly, using triaxial positioning units, with 2μm resolution, it is possible to move the input/output fiber optics. Secondly, since the input fiber optic normally is single-moded, with a core diameter of 4μm, it requires an even more precise positioning, and this is the main reason why using a biaxial piezoelectric-based positioning system, which is placed over the mechanical measuring stages. The piezolectric system is connected to a high voltage power supply, that provides with voltage from 0 to 1500V, which enables having a 300nm resolution in the input fiber

optics positioning. On the other hand, this extremely-accurate positioning system is not generally required in the output fiber optics, since it normally is multimode, with a core diameter of 50μm and thus, its positioning is not so critical. Output fiber optics is directly connected to a photodetector for measuring the power loss in the integrated optical devices. The sample is also on a biaxial measurement stage that allows movement in *x* and *z* axis, that are used when measuring several devices placed on the same chip and when obtaining the reference signal, respectively.

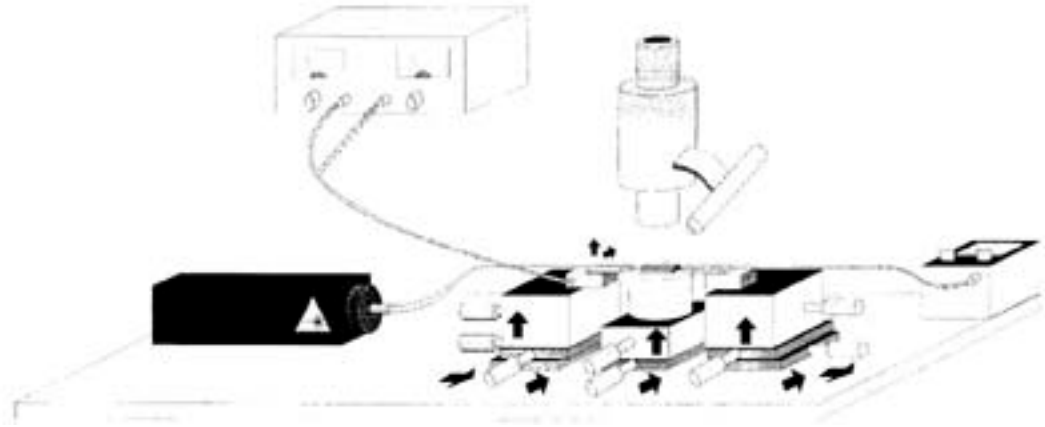

**Fig. 5.1**: Set-up for measuring power losses in integrated optics devices. It consist on two fiber optics, connected to the light source (typically a laser) and to the photodetector. Fibers are positioned by ways of triaxial measurement stages. Input fiber optic has a high precision piezoelectric-based stage. Samples are placed between the fiber and its position is controlled using a biaxial measuring stage system.

As far as light source is concerned, it has to be taken into account that ARROW waveguides were defined so as to have minimum losses at 633nm. This was due to two main factors: the availability of a He-Ne laser source, with 5mW of reference power, and the fact that this wavelength is the most common coherent light source at the visible range.

Measurements as a function of the wavelength can be done simply by replacing the light source by a broad band light source (as could be an halogen lamp) and a visible/IR light monochromator, as shown in fig. 5.2. Light was modulated in intensity with the help of a chopper. Due to the low output power values that are generally obtained when using a broad band light source, a synchronous detection system was used. It consisted on a multimode output waveguide, a silicon PIN or a InGaAs photodetector (for the visible and IR range, respectively) a preamplifier and a

Lock-In amplifier, connected to a PC, where measurements where stored. In turn, the PC controlled the monochromator, allowing the remote wavelength variation. Finally, input fiber optic was replaced by another with 9μm diameter core when measurements in the IR need to be done.

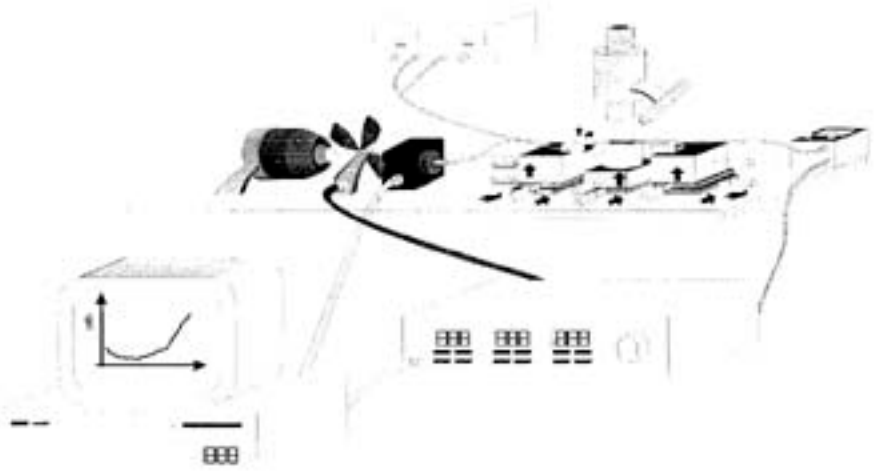

**Fig 5.2:** Experimental setup for losses measurement as a function of the wavelength. Injection system consists on a broad band light source, a chopper and a monochromator. Light is injected to a single mode fiber optic that couples light to the integrated optics device. Detection system is based on synchronous detection and consist on a multimode fiber optic, a silicon PIN (or a InGaAs) photodetector, a preamplifier stage and a lock-in amplifier, connected to a PC.

Finally, near field images were obtained by replacing all the readout system from fig. 5.1 by a x100 microscope objective and a CCD camera connected to a PC, where images are stored.

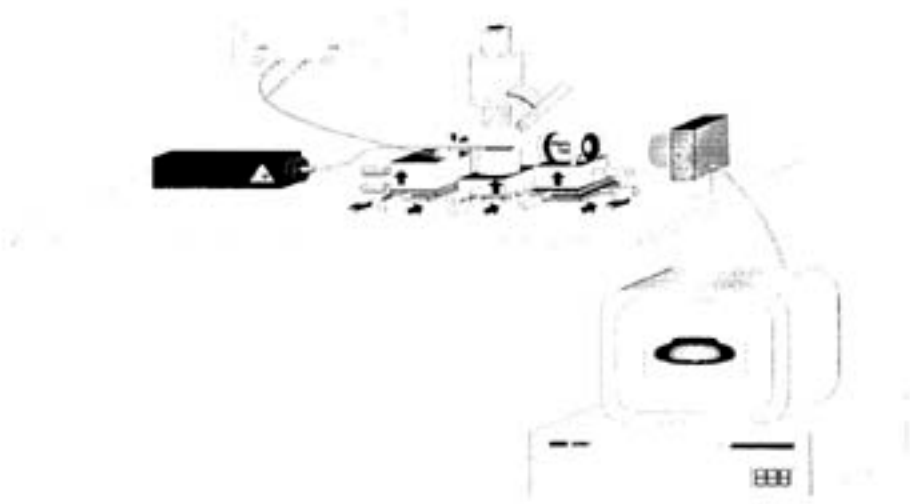

**Fig 5.3:** Experimental setup for the near field detection. x100 microscope objective and CCD camera, connected to a computer, allows obtaining the field profile at the device output.

Once the experimental setups have been presented, the results obtained from the characterization of the integrated optics devices will be shown. It has to be noted that, since all of them are based on ARROW waveguides, the layers needed for obtaining these structures will remain unchanged. Thus, for simplicity, the technological steps that assures obtaining ARROW-A and ARROW-B waveguides are shown in the next subsection. In latter subsections, although the devices would also be based on ARROW configuration, only remarkable steps, as could be using a new mask or an additional layer, will be explained.

## 5.3 Waveguides

### *5.3.1* Rib Waveguides

Although some technological steps for obtaining ARROW-A and ARROW-B waveguides were presented in chapter 3, the whole process for obtaining these structures will be presented again for clarification purposes. As it is shown in table 5.1, the process starts with a one-side polished (100) oriented 4' wafer, in which is grown by wet oxidation at 1000ºC the second cladding layer, with a thickness of 2 µm. This layer is replaced, for ARROW-B, by a silicon oxide film deposited by PECVD at 300ºC with a thickness of 2µm using $SiH_4$ and $N_2O$ as precursors (n=1.56, R=5). First cladding is a 0.38µm LPCVD silicon nitride for ARROW-A obtained at 700ºC, being the precursors ammonia and dichlorsilane. For ARROW-B, this layer is a 0.5µm PECVD silicon oxide, obtained at the same temperature and with the same precursors as the 2$^{nd}$ cladding layer, but with a lower refractive index (n=1.46, R=50). Core layer consists in both cases of a PECVD-deposited silicon oxide, with refractive index n=1.48 (R=7.5) for the ARROW-A and n=1.46 (R=15) for the ARROW-B. This layer is partially etched using RIE in order to assure cross section confinement. It has to be noted that internal asymmetry parameter does not have a zero value. Two main reasons have caused to modify the basic structure. Firstly, a passivation film with a thickness of 2µm is deposited over the core so as to isolate the integrated optics structure from the environment. For both structures this layer is a nearly stoichiometric (n=1.46, R=50)

PECVD silicon oxide. The coincidence of the refractive indexes of the core and the passivation is a major drawback, and only can be overcame by slightly increasing the core refractive index. Although simulations proved that multimode behavior would be obtained even for small variations of $\Delta n_{c2}$, previously obtained experimental results of ARROW-A waveguides with refractive index of 1.48 **[1]**. Actually, they presented better properties as compared to standard ARROW-A, as could be minor losses, shift of the resonant peaks towards larger wavelengths and separation of these peaks as a function of the polarization. Moreover, the modal properties of the waveguides did not suffer a dramatic change to multimode behavior, but it remains being single-moded. This clear discrepancy between theory and experimental is still under study.

| Scheme | Step properties | |
|---|---|---|
| 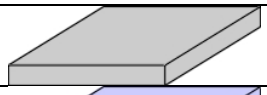 | Silicon substrate. One-side polished, N-type, 4' diameter, 500µm thick | |
| 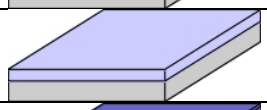 | **A-A** | **2nd cladding:** 2µm wet thermal silicon dioxide. n=1.46 |
| | **A-B** | **2nd cladding:** 2µm PECVD silicon oxide. n=1.56 |
|  | **A-A** | **1st cladding:** 0.38µm LPCVD silicon nitride. n=2.00 |
| | **A--B** | **1st cladding:** 0.5µm PECVD silicon oxide. n=1.46 |
| 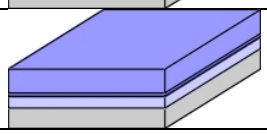 | **A-A** | **Core:** 4µm PECVD silicon oxide. n=1.48 |
| | **A-B** | **Core:** 4µm PECVD silicon oxide. n=1.56 |
| 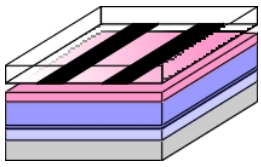 | **CNM-031** mask | |
| | 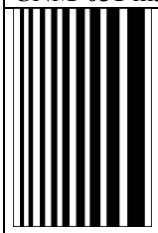 | **Mask:**<br>**Waveguide widths:**<br>1-10µm in steps of 1µm<br>12-20µm in steps of 2µm<br>20-40µm in steps of 5µm<br>**Waveguide lengths:**<br>1-2.5cm µm in steps of 0.5cm |
| | | **Step:**<br>2µm positive photoresist |
| 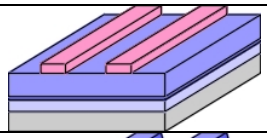 | Exposition: 10sec to UV light<br>Photoresist development | |
| 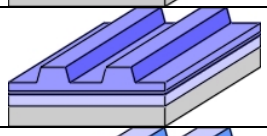 | **Rib definition:** 2.5µm RIE etching with $CHF_3$ | |
| 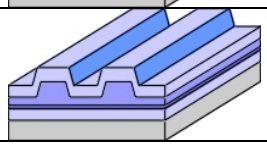 | **Passivation:** 2µm PECVD silicon oxide. n=1.46 | |

| | |
|---|---|
| 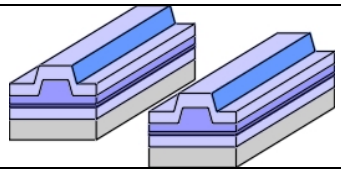 | **Post process:**<br>Cutting by a diamond blade<br>Polishing wit SIC (0.9μm)+ $Al_2O_3$ (0.3μm) |

**Table 5.1:** ARROW-A and ARROW-B fabrication steps.

Experimental results of the total losses as a function of the waveguide width are presented in fig. 5.4. As can be observed, there is a sharp increase as waveguides gets thinner, both in ARROW-A and ARROW-B structures. In previous simulations, this fact was associated to a minor lateral confinement, that is, a decrease on the number of lateral modes as the waveguide width progressively decreases. This assumption has been confirmed by ways of the experimental near field images of ARROW-A waveguides with 1.5μm rib, shown in fig. 5.5, together with the predicted profiles. For wider waveguides, although single mode behavior is obtained in the vertical (i.e. *y* axis) direction, there exists several lateral modes, which where previously labeled as $TE_{0x}$ modes (fig, 5.5a). Concretely, simulations shown in fig. 5.5b confirmed up to four lateral modes. As the waveguide gets thinner, higher order lateral modes reach their cutoff condition and become radiative mode. For waveguides thinner than 8μm, single mode in the cross section is finally obtained, both in experimental (fig. 5.5c) and simulations (5.5d).

As far as total losses is concerned, it could be thought that achieving a value of 3.12dB and 5.23dB for ARROW-A and ARROW-B respectively, is not a promising result. It has to be noticed, however, that within this value, it is taken into account both insertion losses and attenuation, namely

$$P_{out} = P_{in} - LP_{att} - P_{ins} \tag{5.1}$$

where $P_{out}$ and $P_{in}$ are the power at the output and at the input, respectively, L the waveguide length, $P_{att}$ stands for the attenuation and $P_{ins}$ are the insertion losses. From the previous expression, it is possible to know the attenuation if two identical waveguides with different length ($L_1$ and $L_2$) are measured, using

$$P_{att} = \frac{P_{out,1} - P_{out,2}}{L_2 - L_1} \tag{5.2}$$

Finally, since insertion losses do not depend on the total length of the device, they can also be known considering

$$P_{ins} = \frac{(P_{out,1} - P_{at}) + (P_{out,2}L_1 - P_{out,1}L_2)}{2} \tag{5.3}$$

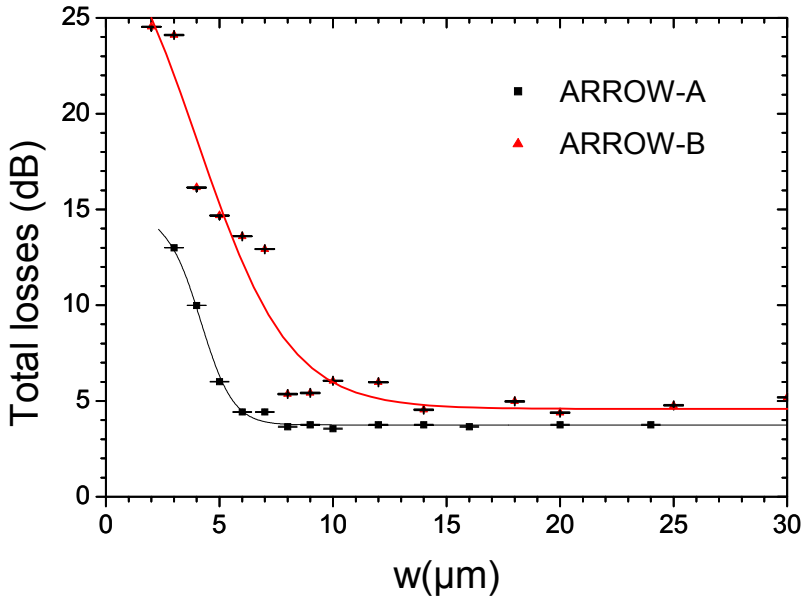


**Fig 5.4:** Total losses as a function of the waveguide width for ARROW-A and ARROW-B structures.

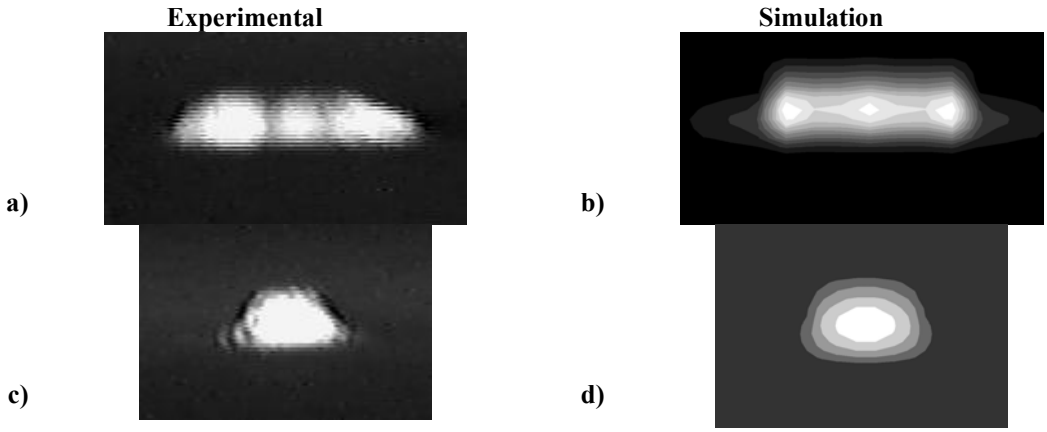


**Fig 5.5:** Field profiles for ARROW-A waveguides with 1.5μm rib, where several lateral modes are observed experimentally (a) and by simulation (b) on the wider waveguides. For structures with width less than 8μm, measured (d) and predicted (d) field profile predicted single mode behavior.

Two identical sets of waveguides, with lengths of 1 and 1.5cm were measured. With the help of the previous expressions, it was stated that both structures showed an identical behavior in attenuation being their values lower for ARROW-A structures.

Thus, for simplicity, only results for ARROW-B are presented in fig. 5.6, together with the predicted values. It can be seen that above a given width value, attenuation becomes nearly independent of the waveguide width, with a value of 1.62dB/cm (ARROW-A presented an attenuation of 0.45dB/cm). Although experimental and simulation results show the same tendency, there exists a difference of an order of magnitude between them. This mismatch between theory and measurements could be associated to impurities on the core layer, excessive wall roughness or non-vertical walls. From expression 5.3, it was possible to determine the insertion losses that were 2.2±0.2dB for ARROW-A and 2.5±0.2dB for ARROW-B.

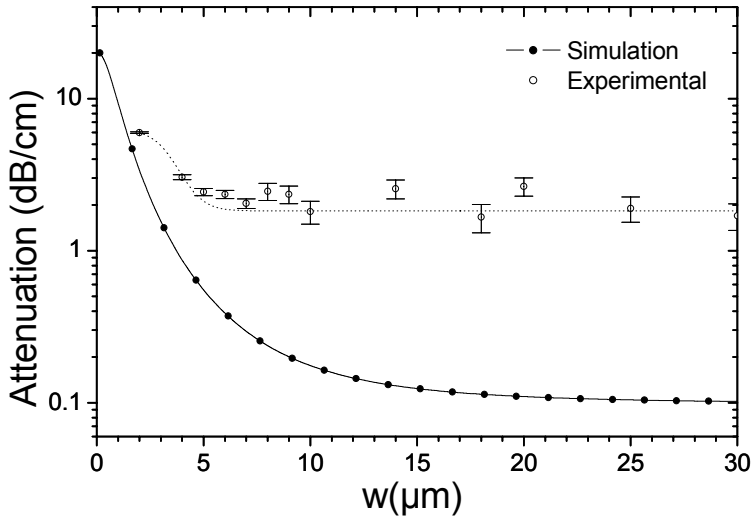


**Fig 5.6:** Experimental results and simulation of the attenuation as a function of the waveguide width for ARROW-B structures.

Once the attenuation was measured, the response in wavelength for 20μm width ARROW-A and -B structures was obtained (fig. 5.7). This behavior is of extreme importance in ARROW waveguides because the antiresonant pair is tuned at the working wavelength (633nm). Thus, if the minimum losses are not located at this working wavelength, it would be a clear sign that there has been an error either in the design or in the structure fabrication steps. As can be seen, maximum power at the output is obtained at 630nm for ARROW-A and 610nm for ARROW-B. The small discrepancy in the latter structure can be associated to a minor uniformity of the PECVD-deposited layers as compared to silicon oxidation or LPCVD, which could

cause a small displacement from the working wavelength. Nevertheless, this result allows confirming the ARROW structure robustness: although probably exists a small variation with the fabrication parameters, the power obtained at 610nm differ much less than 5% of the power obtained at the working wavelength.

On the other hand, the increase of the attenuation as the wavelength increases is due to a progressive detuning of the antiresonant layers, which progressively changes its operation regime, form antiresonance to resonance, enhancing transmission to the substrate. Finally, the total losses increase at low wavelengths is due to the radiative behavior of the 1st order mode of the injection fiber, since at these wavelengths, and due to the position and length of the input fiber optics, it is not single-mode.

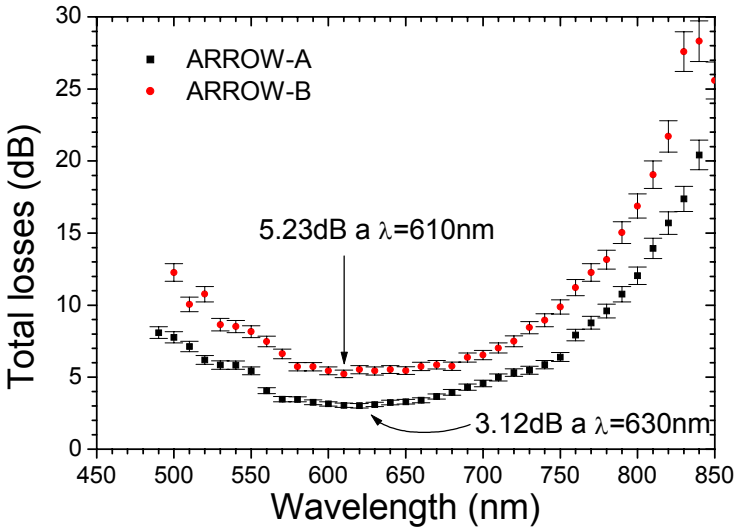


**Fig 5.7:** Total losses as a function of the wavelength for ARROW-A and ARROW-B structures.

ARROW structures have been characterized in power and wavelength. Although some discrepancies have been observed between theory and experimental, results show the appropriateness of the fabrication technology. Moreover, the relative low losses for both waveguides opens two opposite research fields: As far as PECVD is concerned, obtaining more homogeneous and impurity-free layers, while keeping the possibility of vary the refractive index would be an extremely useful and powerful in optoelectronics. On the other hand, with the available technology, it is possible to fabricate all previously designed structures, with acceptable power losses.